

JGR Space Physics

RESEARCH ARTICLE

10.1029/2024JA032767

Key Points:

- The meteor speed peaks northward in the local morning and shifts clockwise to southward by local evening
- Meteor speed distribution has two Gaussian peaks at ~28 and ~54 km/s, revealing semi-annual and annual variation cycles respectively
- Major meteor showers occur with 45%–97% higher counts than the background, and are associated with increases in the peak speeds

Correspondence to:

W. Yi and X. Xue,
yiwen@ustc.edu.cn;
xuehx@ustc.edu.cn

Citation:

Wu, K., Yi, W., Xue, X., Reid, I. M., & Lu, M. (2024). Diurnal and seasonal variations of meteor speed and arrival angle observed by Mengcheng meteor radar. *Journal of Geophysical Research: Space Physics*, 129, e2024JA032767. <https://doi.org/10.1029/2024JA032767>

Received 18 APR 2024

Accepted 18 SEP 2024

Author Contributions:

Conceptualization: Koutian Wu
Data curation: Koutian Wu, Maolin Lu
Formal analysis: Koutian Wu
Funding acquisition: Koutian Wu, Xianghui Xue
Investigation: Koutian Wu
Methodology: Koutian Wu
Project administration: Xianghui Xue
Resources: Xianghui Xue
Software: Koutian Wu, Maolin Lu
Supervision: Xianghui Xue
Validation: Koutian Wu
Visualization: Koutian Wu
Writing – original draft: Koutian Wu
Writing – review & editing: Koutian Wu, Xianghui Xue, Iain Murray Reid

Diurnal and Seasonal Variations of Meteor Speed and Arrival Angle Observed by Mengcheng Meteor Radar

Koutian Wu^{1,2,3} , Wen Yi^{1,2} , Xianghui Xue^{1,2,4} , Iain Murray Reid^{5,6} , and Maolin Lu^{1,2} 

¹CAS Key Laboratory of Geospace Environment, School of Earth and Space Sciences, University of Science and Technology of China, Hefei, China, ²CAS Center for Excellence in Comparative Planetology, Anhui Mengcheng Geophysics National Observation and Research Station, University of Science and Technology of China, Hefei, China, ³X-Institute, Shenzhen, China, ⁴Hefei National Laboratory, University of Science and Technology of China, Hefei, China, ⁵ATRAD Pty Ltd., Underdale, SA, Australia, ⁶School of Physics, Chemistry and Earth Sciences, University of Adelaide, Adelaide, SA, Australia

Abstract Meteor speed is crucial in identifying key astronomical aspects of the meteoroid environment, including the influx of meteoric material and the distribution of meteoric radiants. This study investigates diurnal and seasonal variations of meteor speed from April 2014 to December 2023 observed by the Mengcheng meteor radar (MCMR; 33.4°N, 116.3°E). In addition to the expected diurnal variation of meteor speed, azimuth peak, zenith peak, and the azimuthal direction of maximum meteor speed due to the Earth's rotation, where the meteor speed peaks northward in the local morning and shifts clockwise, we find that the meteor speed distribution resembles a superposition of two Gaussian distributions, with the lower (higher) distribution mainly ranging from 20 to 40 (45–65) km/s. The two speed peaks are estimated using a double-Gaussian fitting approach. In terms of seasonal variation, we find that (a) the low-speed peak indicates a semi-annual variation cycle, with maxima in June–July and December–January, and minima in February and August; (b) the high-speed peak indicates an annual variation cycle, with maxima in September–December and minima in March. There is also a correlation between the seasonal variations in the meteor speed peaks and the occurrence of meteor showers. Statistical analysis provides a map of seasonal variations in the intensity, duration, and timing of meteor shower activities, which is supplemental to previous shorter-duration studies using backscatter meteor radar observations. We also find notable shower events where the meteor counts exceed 45%–97% of the background count on corresponding event dates and speeds.

Plain Language Summary Meteor speed plays a crucial role in understanding the quantity and distribution of meteoroids in our environment, yet there are limited observations and investigations conducted at mid-latitudes. In this study, we utilized a meteor radar located in Mengcheng (in the northern lower middle latitudes) to investigate diurnal and seasonal variations in meteor speed from April 2014 to June 2023. Our findings revealed that meteor speed is generally faster in the morning and slower in the afternoon and evening, and the angle of arrival of meteors varies with local time. Additionally, we discovered that meteor speed exhibits two peaks, with the lower one at about 28 km/s and the higher one at 54 km/s. Seasonal changes indicated a semi-annual variation cycle in the low-speed peak and an annual variation cycle in the high-speed peak. Furthermore, we observed several noteworthy meteor showers and their interannual variations.

1. Introduction

Meteoroids are small particles that enter the Earth's atmosphere at high speeds, creating plasma density enhancement trails detectable by radar as radio meteors and also optically as “meteors” when they generate light. They typically occur at altitudes below 130 km where the air is dense enough to burn and ionize their surface layers (Ceplecha et al., 1998; Ryabova et al., 2019). Once formed, the ionized trails drift with the local wind and diffuse into the background atmosphere. The diffused meteor material, which contains some metal atoms, precipitates into the atmosphere and is moved downward. It has been quite challenging to determine with accuracy just how much meteoric material enters the Earth's atmosphere. Older values range between 5 and 300 tonnes per day (Brown et al., 2002; Ceplecha, 1992). More recently, Drolshagen et al. (2017) estimated that 54 tonnes of extraterrestrial debris (interplanetary dust, meteoroids, or asteroids) fall to Earth every day, while Carrillo-Sánchez et al. (2020) estimated daily values of meteoroid flux from 15 to 60 tonnes. However, what is clear is that the highest mass influx is caused by meteoroids with sizes between a few tens of microns and 1 mm.

The influx of meteoric material affects the chemistry of the atmosphere, the production of aerosols, and the productivity of the oceans, which has prompted more studies to comprehend the variation of the influx of interplanetary dust (Rudraswami et al., 2021). The meteoric deposition also results in layers of free neutral metal atoms in the mesosphere/lower thermosphere (MLT) (~ 80 – 110 km), which are readily detected using ground-based lidars (see e. g., Bowman et al., 1969). The vapourized material due to meteors also leads to the formation of sporadic *E* layers, which consist of metallic ions at ionospheric *E* region heights, and are particularly important for radio-wave propagation (see e.g., Maruyama et al., 2008). Meteor plasma trails can also generate plasma instabilities in the ionosphere (Dou et al., 2010; Kelley, 2004; Oppenheim & Dimant, 2006). As a result, studying the meteoroid flux and its seasonal change is crucial for advancing our understanding of its impact on our natural environment.

Radar has been used to routinely detect meteor trails since shortly after the Second World War (see e.g., Reid, 2024; Reid & Younger, 2016). Fainter meteors that result from meteoroids in the sub-mm size range are typically detectable by radar surveys. The sort of echo that different radars can detect (meteor head echo vs. trail echo, for example) and the size range depend heavily on the transmitted power and system aperture (see e. g., Janches et al., 2014, 2015). Large data sets are typically produced because the number of meteoroids identified by a single radar station far outnumbers the more infrequently detected optical meteors. Moreover, radar surveys can run continuously throughout the day, allowing for the observation of meteors coming from the Helion source. Meteor radars have some advantages that other sensor systems do not have. As long as there are ionized meteor trails available for observation, meteor radars may function day or night, in any weather, unlike optical observations, rockets, and satellites. Because of this, meteor radars may be used to detect a continual stream of cosmic debris regardless of the time of day or the weather (Marino et al., 2022; Younger, 2011).

Drolshagen et al. (2020) reviewed previous studies of meteoroid speed distributions, including those derived from the Harvard Radio Meteor Project, 1968–69 Synoptic Year Program. The most complete of these is by Taylor and Elford (1998) who reanalyzed the orbital element distributions of the detected meteoroids to correct for several potential biases including the observation times, the radar antenna beam patterns, and the radar detectability of the meteoroid and the characteristics of the atmosphere. They presented the resulting radiant distribution for meteoroids with masses greater than 10^{-4} g encountering the Earth. This shows the six radiant sources as the Helion, Anti-Helion, North Toroidal, South Toroidal, North Apex, and South Apex. Subsequent work by Galligan and Baggaley (2004) using the Advanced Meteor Orbit Radar found similar orbital distributions but slightly larger speeds. We note that Drolshagen et al. (2020) point out that both optical and radar studies of meteoroids are biased against smaller slower meteoroids and go on to focus on meteoroids larger than 1 g in their work.

To accurately determine the orbit of meteor streams, it is crucial to have precise knowledge of the speed of shower meteors toward Earth (Younger et al., 2012). Holdsworth et al. (2008) analyzed the seasonal variation of meteor speed observed by the Davis meteor radar in Antarctica and found that the meteor speed distribution peaks at around 25 km/s. The form of the distribution they found did not change much throughout the year, except for a secondary peak that can be seen at around 55 km/s, with its center around early March. Singer et al. (2004) reported the meteor flux and speed observed by the meteor radar located in Juliusruh (54.6°N , 13.4°E) and at the ALOMAR observatory on Andøya (69.3°N , 16.0°E) in the Arctic and found that the meteor count in June showed a significant peak and that the meteors detected may have originated from sporadic meteoroids with large ecliptic inclinations and low to moderate atmospheric entry speeds.

A study of diurnal and seasonal variation of meteoric flux at the South Pole using a VHF meteor radar was carried out by Janches et al. (2004), who found that as there is an asymmetry in the flux recorded at both poles, showing it is likely that the majority of meteoric activity is centered on the ecliptic plane and is more observable during the polar summer season. J. P. Younger et al. (2009), P. T. Younger et al. (2009) investigated the distribution of meteor sporadic radiant observed by meteor radars in the Arctic, Antarctic, and near the Equator, and found that the observed meteor counts showed dependence on latitude and time. This dependence is likely due to multiple factors, including the distribution of sporadic radiant, yearly fluctuations in atmospheric density, and the radar's sensitivity toward meteors originating from varying source elevations, in addition to the background temporal and spatial changes in meteor flux. Li et al. (2022) reported short-duration meteor showers at Mohe (53.49°N), Beijing (40.3°N), Wuhan (30.54°N), and Ledong (18.44°N) in China. However, long-term observation and investigations of meteor speed and their seasonal variation characteristics at midlatitudes are scarce (Hindley, 2022; Hindley et al., 2022).

Table 1
The Main Operational Characteristics of the Mengcheng Meteor Radar

Frequency	38.9 MHz
Peak power	24 kW at the transmitter
Pulse repetition frequency	430 Hz
Transmission mode	Circular
Coherent integrations	4
Range resolution	1.8 km
Pulse type	Gaussian
Pulse width	24 μ s
Duty cycle	15%
Detection range	70–110 km

Therefore, more than 9 years of observations using the meteor radar is a supplement for meteoric observation at mid-latitudes. The goal of this study is to introduce meteor speed observation by the University of Science and Technology of China (USTC) meteor radar at Mengcheng station. This paper is structured as follows. In Section 2, we introduce the observational instruments and data sets. In Section 3, we present the diurnal variations of meteor speed and angle of arrival (azimuth and zenith). In Section 4, we perform an analysis of the seasonal variation of the meteor speed's double-Gaussian distribution. Lastly, we offer a summary of our findings and draw our conclusions.

2. Instruments and Data Sets

The speed distributions of meteors and their seasonal variation are investigated in this study using data obtained from the USTC Mengcheng meteor radar (MCMR) from April 2014 to June 2023. The USTC MCMR, which is

part of the ATRAD Enhanced Meteor Detection Radar (EMDR) series, is located in the lower northern middle latitudes of China and is specifically situated in Mengcheng (33.36° N, 116.49° E). It is analogous to the Buckland Park meteor radar system reported by Holdsworth et al. (2004), and in this study, we use underdense meteor echos (i.e., error code = 0) for analysis. The radar, which was put into operation in April 2014, has been working with 24 kW for transmitting. Five two-element Yagi antennas composing a cross “+” shape arrangement are used for reception. By examining the phase drift of echoes from underdense meteor trails, the radar is primarily used to determine winds in the MLT region (Yi et al., 2023). Table 1 provides a summary of the main operational characteristics of the MCMR.

By employing simple interferometry, signals captured from several antenna pairs were auto- and cross-correlated to determine the radial speed, altitude, zenith, and azimuth angles for each meteor echo (Jones et al., 1998). The information to detect the meteor's position in the sky with an angular precision of higher than 2° and a range resolution of 1.8 km is provided by interferometric analysis of the received meteor signal.

A basic overview of the meteor echoes observed by the MCMR is shown in Figure 1. As shown in Figure 1a, which displays the horizontal projection of 12,337 meteors recorded by MCMR on 2 October 2022, meteors are detected in all horizontal directions and mostly in the daytime (see Figure 1e for color scale). The backscattered echoes are seen in a 300 km radius around the MCMR, most of which are located between 50 and 150 km away. Figure 1b presents the local time distribution of meteor echoes observed on 2 October 2022, by the MCMR. As evident from the figure, the meteor count exhibits a distinct diurnal variation, higher during the morning (i.e., 0–12 local time, or LT for short) and lower from the local afternoon until midnight (i.e., 12–24 LT). According to Figure 1c, the meteor echoes are observed within an altitude range of around 70 and 110 km, with a peak height of 90.00 km and a width of 5.575 km. The neutral density affects the meteor distribution's peak height, which can fluctuate seasonally by a few kilometers which will be presented in Figure 2. The zenith angles are predominantly dispersed between 45° and 70° and up to 80° from the zenith (Figure 1d), which shows good accordance with Singer et al. (2004), who indicated that a considerable portion of the meteor trail echoes at elevation angles at 35° or less. The reduced occurrence rates near the 90° and 270° azimuths may stem from limited visibility due to landscape and obstacles. Additionally, inherent attributes of meteor showers such as temporal variations, contribute to this phenomenon. The azimuth distribution of meteors is shown in Figure 1e. The azimuth angles are rather well distributed, with a somewhat higher concentration to the north of the receivers (i.e., 350° – 20°).

Figure 2 displays the seasonal variation of three parameters measured by the MCMR from April 2014 to June 2023: (a) the daily count, and (b) the peak and width of meteor height distribution on 2 October 2022. In this study, days with a meteor count below 1,000 were excluded to minimize possible errors associated with low meteor counts. Although there are minor data gaps mainly due to site maintenance, the MCMR has consistently exhibited a high ability to detect meteor velocities at lower mid-latitudes.

Figure 2a displays the seasonal variation in the meteor counts observed by the MCMR at the northern lower midlatitude, which exhibits a seasonal variation with a maximum in mid-fall, relatively stable values from January to April, and a minimum in late May. Since the radar commenced gathering data, the daily meteor detection count

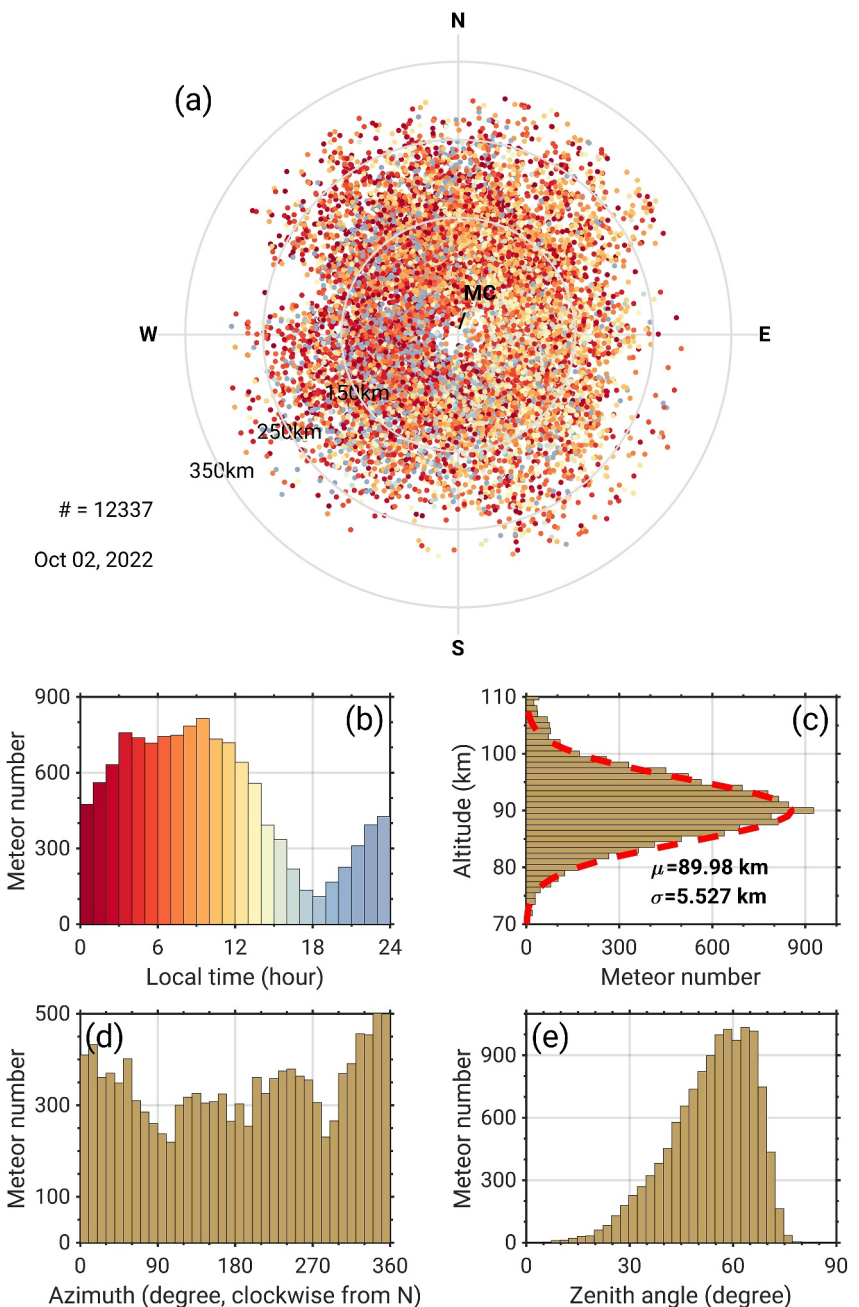


Figure 1. The meteor distribution map for 2 October 2022, is shown in panel (a), and the color of each echo is denoted by its corresponding detection in local time, as shown in the color scale in panel (b). The (c) altitude, (d) zenith, and (e) azimuth of meteor echo distributions were observed by the MCMR on 2 October 2022.

has typically ranged from 6,000 to 20,000. Changes in the observation location of the main sporadic meteor sources in space seasonally are primarily responsible for this variation (Campbell-Brown, 2008).

The meteor count basically shows an annual variation cycle in the Northern and Southern Hemispheres, except for the season of peak meteor count varies with latitudes. For example, at Davis Station (68.6°S , 77.9°E) in Antarctica, meteor counts show a maximum in January and a minimum in August (Yi et al., 2017). Also, at Svalbard (78.3°N , 16°E) and Tromsø (69.6°N , 19.2°E) meteor radar located in the Arctic, meteor counts show a maximum in July and a minimum in February (Yi et al., 2021). Singer et al. (2004) reported that meteor counts at Juliusruh (54.6°N , 13.4°E) and ALOMAR (69.3°N , 16.0°E) both show the largest values in June and the lowest

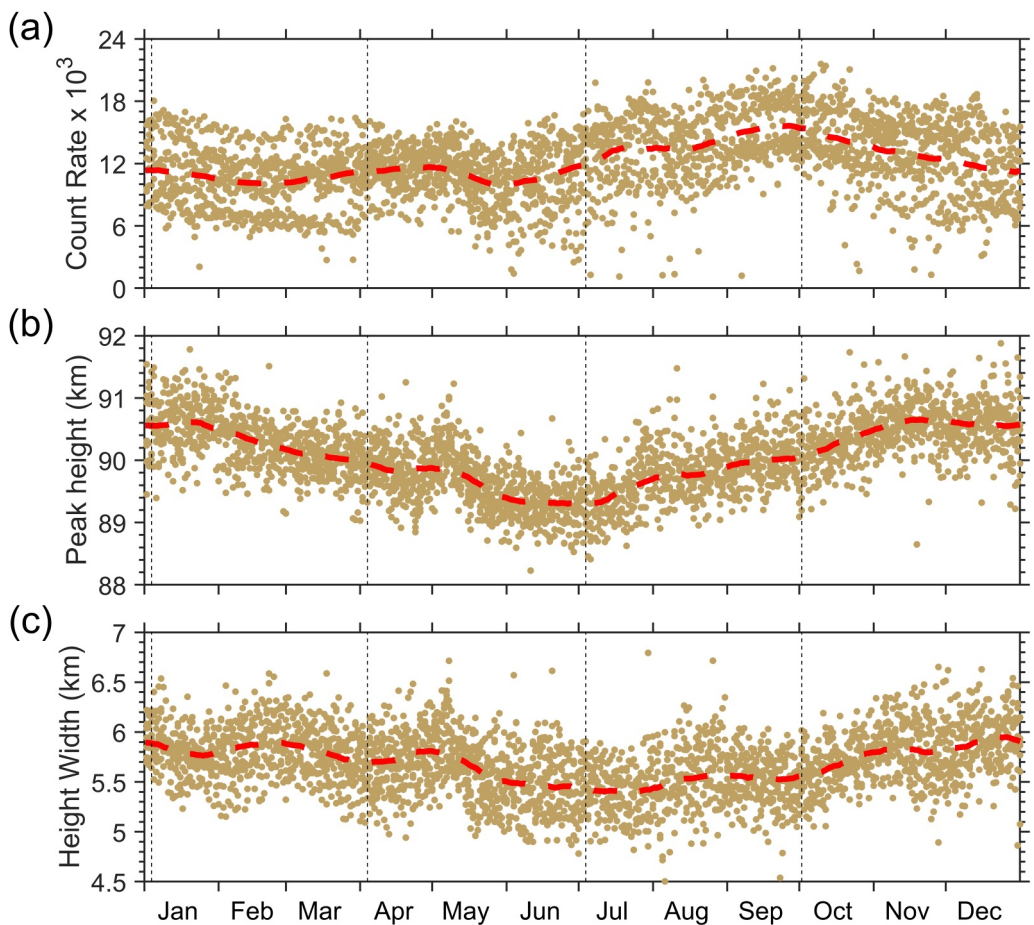


Figure 2. Annual composite of (a) the daily count, (b) the peak height, and (c) the width of height distribution of meteor echoes observed by the MCMR from April 2014 to June 2023. The red line denotes the 30-day smoothed mean value of the daily count, while the black dashed lines denote the four dates displayed in Figure 3.

in February. Additionally, meteor radar in the northern middle latitudes, specifically Mohe (53.5°N , 122.3°E) and Beijing (40.3°N , 116.2°E), presented relatively weak seasonal variations with maxima in September and October and minima in February and March, respectively (Yi et al., 2021). Yi et al. (2018) reported that the meteor counts observed by the Kunming meteor radar at northern low latitudes (25.6°N , 108.3°E) exhibit an annual variation cycle, peaking in July and minima in late March. However, Janches et al. (2004) and Reid et al. (2006) found that meteor counts at southern high latitudes peaked in January and peaked in June. The Earth's orbital position in relation to sporadic meteor sources, the radar's sensitivity to meteors from various source altitudes, and the location of the observation site all contribute to the annual variation cycle of the counts (J. P. Younger et al., 2009; P. T. Younger et al., 2009).

In Figure 2b, the peak height observed by the MCMR shows an annual variation cycle, with a maximum value of approximately 92 km in winter and a minimum value of approximately 88.5 km in summer. The width of meteor distribution fluctuates from 4.5 km in summer to 6.5 km in winter. The peak height of meteor distribution can be used to indicate variations in mesospheric density, but it is also affected by seasonal variations in meteor speed (e.g., Yi et al., 2017, 2018). The peak height in Davis Station (68.6°S) mainly shows an annual variation cycle, reaching its maximum in summer (January) and minimum in winter (July). Similarly, the meteor radar located in the Arctic stations of Svalbard (78.3°N) and Tromsø (69.6°N) displays peak heights that primarily follow an annual variation with an additional semiannual variation. The maximum peak height occurs in fall (October) while the minimum height is observed in spring (February). The peak altitude at Mohe (53.5°N) (higher northern midlatitudes) indicates a semiannual oscillation and a relatively weak annual oscillation. At northern mid-latitudes, the peak height in Beijing (40.3°N) mainly exhibits annual variations, with the highest peak height

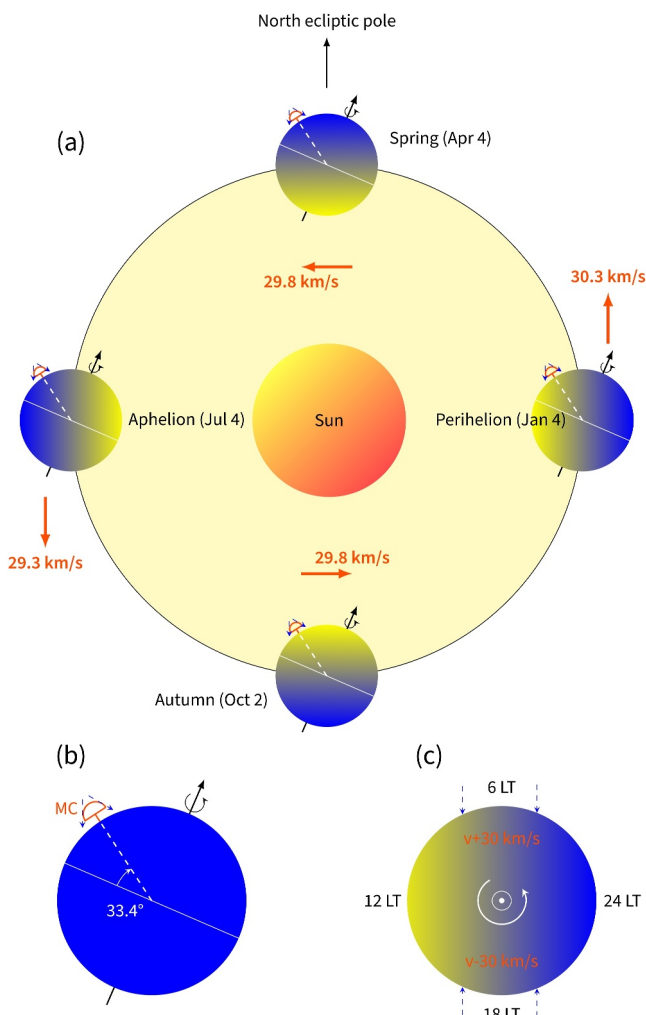


Figure 3. Schematic of the MCMR viewing geometry. (a) MCMR's position in the solar system changes due to Earth's rotation and orbit around the Sun; (b) MCMR location on Earth; (c) Viewing geometry of MCMR varies with local time, affecting observed meteor speed and angle of arrival, viewed from the North Ecliptic Pole.

The meteor radar's direction toward the primary source region of meteors varies with the rotation of the Earth, which has a period of 1 day, causing the azimuth peak to change in a clockwise manner while causing the zenith peak to increase in the morning and decrease in the afternoon and evening. These results are consistent with Lau et al.'s (2006) model of Earth's rotation.

Figure 6 illustrates the diurnal variations in meteor height and speed over 30 days. The MCMR records a distinct diurnal variation in meteor speed, showing higher speed in the local morning (0–12 LT) and lower speed from the local afternoon to midnight (12–24 LT). This phenomenon occurs due to the Earth's rotation (see Figure 3c) and is well-explained by Sugar (1964): On the morning side of Earth, meteors are swept up by Earth's forward motion as it orbits the Sun. Conversely, on the evening side, only meteors that overtake the planet are able to reach it. This uneven distribution leads to a peak occurrence rate and maximum speed at approximately 6 LT and a trough in occurrence rate and minimum speed at around 18 LT. The degree of variation in this ratio is contingent on the observer's latitude. Kero et al. (2012) reported that the diurnal detection rate exhibits an asymmetrical seasonal variation near the equinoxes. The months preceding the Spring equinox (around 20 March) exhibit higher daily maxima and overall diurnal numbers, compared to the subsequent months.

recorded in fall (October–November) and the minimum during summer (July) (e.g., Liu et al., 2016; Yi et al., 2021).

Figure 3 is a schematic illustrating the viewing geometry of the MCMR. The points highlighted are perihelion (4 January 2022), aphelion (4 July 2022), and the equinoxes between them (4 April 2022, and 2 October 2022, in spring and fall, respectively). In Section 3, we primarily concentrate on these four positions in the Earth's orbit to analyze the variation of meteoroid fluxes along the Earth's route about the Sun.

3. Diurnal Variations of Meteor Speed and Angle of Arrival (Azimuth and Zenith)

Figure 4a shows the diurnal variation of the meteor azimuth observed by the MCMR during 1–3 October, 2022. The data is processed using a running mean with a 3-hr window to provide a minimal amount of smoothing. Figures 4b–4e show the 30-day composite diurnal variation of meteor azimuth centered on four selected dates. Figure 5 shows the diurnal variation of the meteor zenith observed by the MCMR. As shown in Figure 5a, the zenith distributions generally reach their maxima at 60°–70°. In Figures 5b–5e, the zenith angles observed by the MCMR are generally stable at about 60°–70°, except at 14–18 LT, the zenith angle decreases significantly to 45°.

In general, the change in the azimuth direction with the highest number of meteors (or azimuth peak) occurs in a clockwise manner. Specifically, the direction of the azimuth peak changes from the northwest (270–360°) to the northeast (0–90°) during the local morning (0–12 LT), while during the local afternoon to evening (12–24 LT), the direction of azimuth peak changes from the southeast (90–270°) to the southwest (180–270°). On the other hand, the meteor zenith angle also exhibits a strong diurnal variation. More precisely, the zenith direction with the highest number of meteors (or zenith peak) increases during the local morning (0–12 LT) but decreases during the local afternoon to evening (12–24 LT). Additionally, while the meteor zenith demonstrates a concentrated distribution between 0 and 12 LT, it tends to display a more dispersed distribution during 12–24 LT, reaching its utmost scatter around 18 LT.

From Figures 4b–4e and 5b–5e, these diurnal variations of meteor angle of arrival (azimuth and zenith) are consistent throughout the year and are primarily attributed to the counterclockwise rotation of the Earth (see Figure 3c).

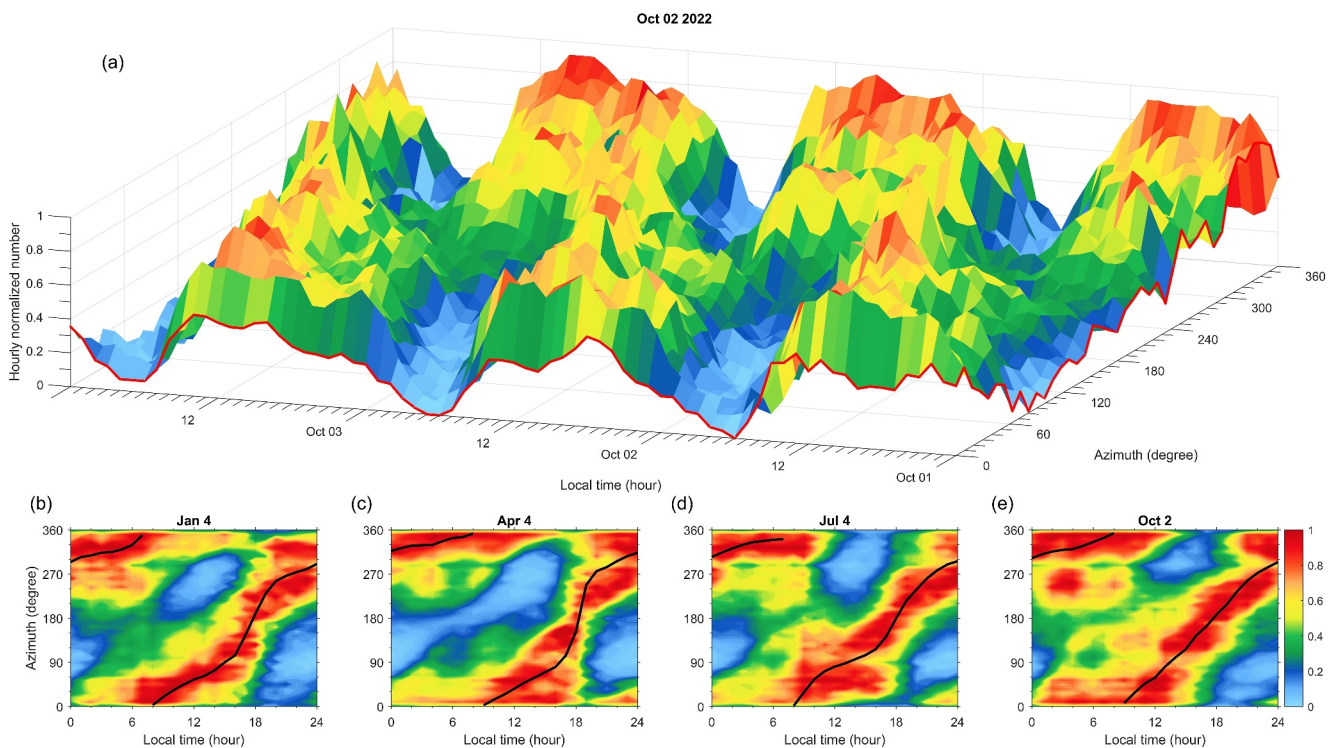


Figure 4. (a) Diurnal variation of meteor azimuth distribution from 1 October to 3 October 2022 (3-hr running mean), with red lines showing local time distribution of meteors at 0 azimuth and azimuth distribution at 0 local time. (b–e) Diurnal variation of meteor azimuth distribution, 30-day composite centered on from 4 January to 2 October 2022. Meteor counts are hourly normalized to the maximum count. Black lines indicate azimuth peak variations corresponding to local time.

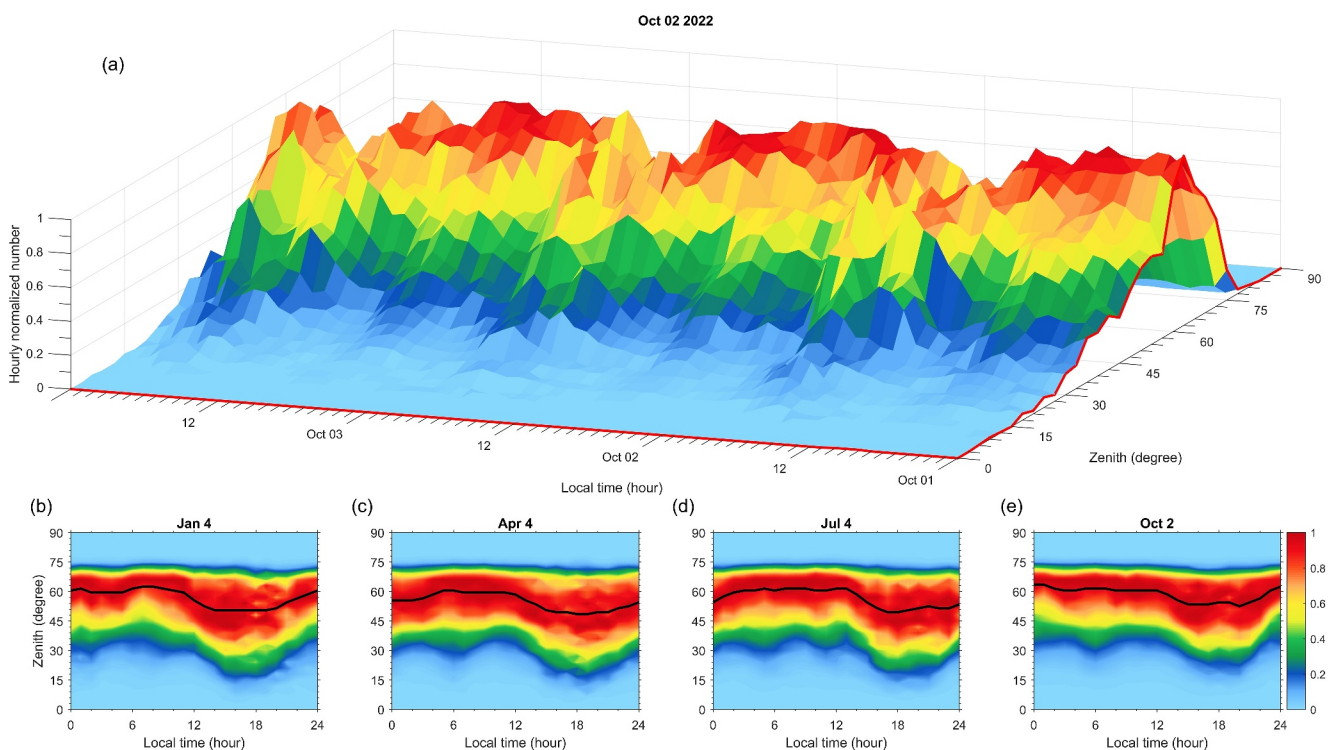


Figure 5. Same as Figure 4, but for meteor zenith angle.

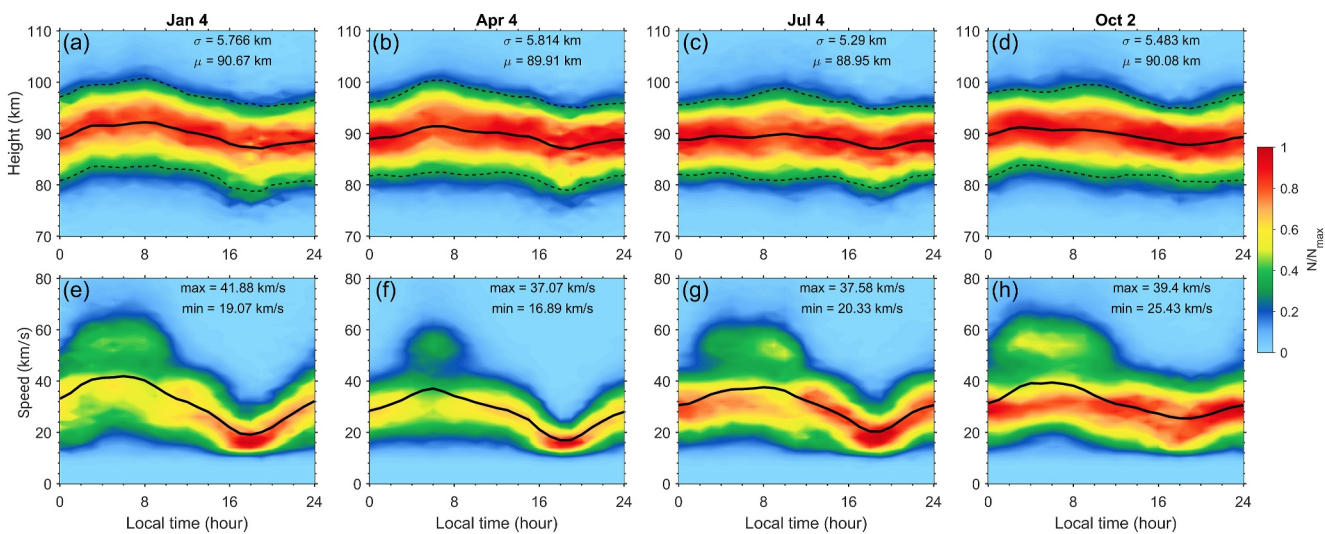


Figure 6. The 30-day composite of diurnal meteor height and speed variations centered on 4 January to 2 October 2022 (columns 1–4), respectively. Top row (a–d): Diurnal variations of meteor height. Black lines and dashed lines denote the peak and width of height distribution in local hours, labeled on the top right. Bottom row (e–h): Diurnal variations of meteor speed. Black lines show mean hourly meteor speeds, with maximum and minimum labeled on the top right. Meteor counts are hourly normalized to the maximum count.

Meteors travel at varying speeds when entering the Earth's atmosphere. The meteor detection altitudes are influenced not only by their speeds but also by other factors such as the vertical distribution of background atmospheric density and temperature. However, the speeds largely influence the altitude ranges in which they can be detected. Rapid-moving meteors quickly burn up into plasma, leaving a detectable trail at higher altitudes. Slow-moving meteors burn up more gradually and can only be detected at lower altitudes. Thus, meteor altitude decreases at 18 LT following a decrease in meteor speed. The maximum meteor altitudes are found with the fastest meteors, whereas the slowest meteors produce lower altitudes.

In addition, Figure 6 reveals that there is a seasonal variation in meteor height and speed. The peak height on four selected days generally followed the results shown in Figure 2b, which indicates higher peak height in winter and lower peak height in summer, which is described in Yi et al. (2019). Moreover, Figures 6e–6h identified the 30-day period centered on 4 January and 4 July to be when there are the largest and smallest changes in meteor speed, respectively. It is important to acknowledge that the diurnal variations of atmospheric density can play a significant role in changes in meteor altitude. It can be complex to distinguish the effects of atmospheric density and meteor speed in such changes. While the acceleration of a meteor can provide insight into changes in atmospheric density, it is not within the scope of this study and will be investigated further in future work.

These findings show that there exist variations in the azimuth, range, altitude, and speed of meteors. To better examine the relationship between meteor azimuth and meteor speed, the collected data was partitioned into 3-hr intervals based on local time (ranging from 0 LT–3 LT to 21 LT–24 LT), and subsequently plotted in Figure 7. Notably, the direction of the maximum speed exhibited a clockwise rotation with increasing time. To quantify this directional tendency, we computed a vector, denoted as \mathbf{Q} , using Equation 1 similar to that described in Hocking (2004):

$$\mathbf{Q}(t_1, t_2) = \langle v_i \cos \phi_i \rangle \mathbf{e}_x + \langle v_i \sin \phi_i \rangle \mathbf{e}_y \quad (1)$$

where v_i and ϕ_i denote the speed and azimuth angle of the i -th meteor, respectively, and $\langle \rangle$ denotes an ensemble average. \mathbf{Q} is formed by this average, pointing toward the predominant/general direction of the higher values of v , indicating the average direction of the maximum meteor speed.

\mathbf{Q} is also illustrated in Figure 7, distribution maps of meteor speeds as a function of horizontal distance and azimuth. In general, there is a clockwise change in the direction of \mathbf{Q} . Specifically, during the local morning (0–12 LT), the direction changes from the northwest (270° – 360°) to the northeast (0° – 90°), while during the local

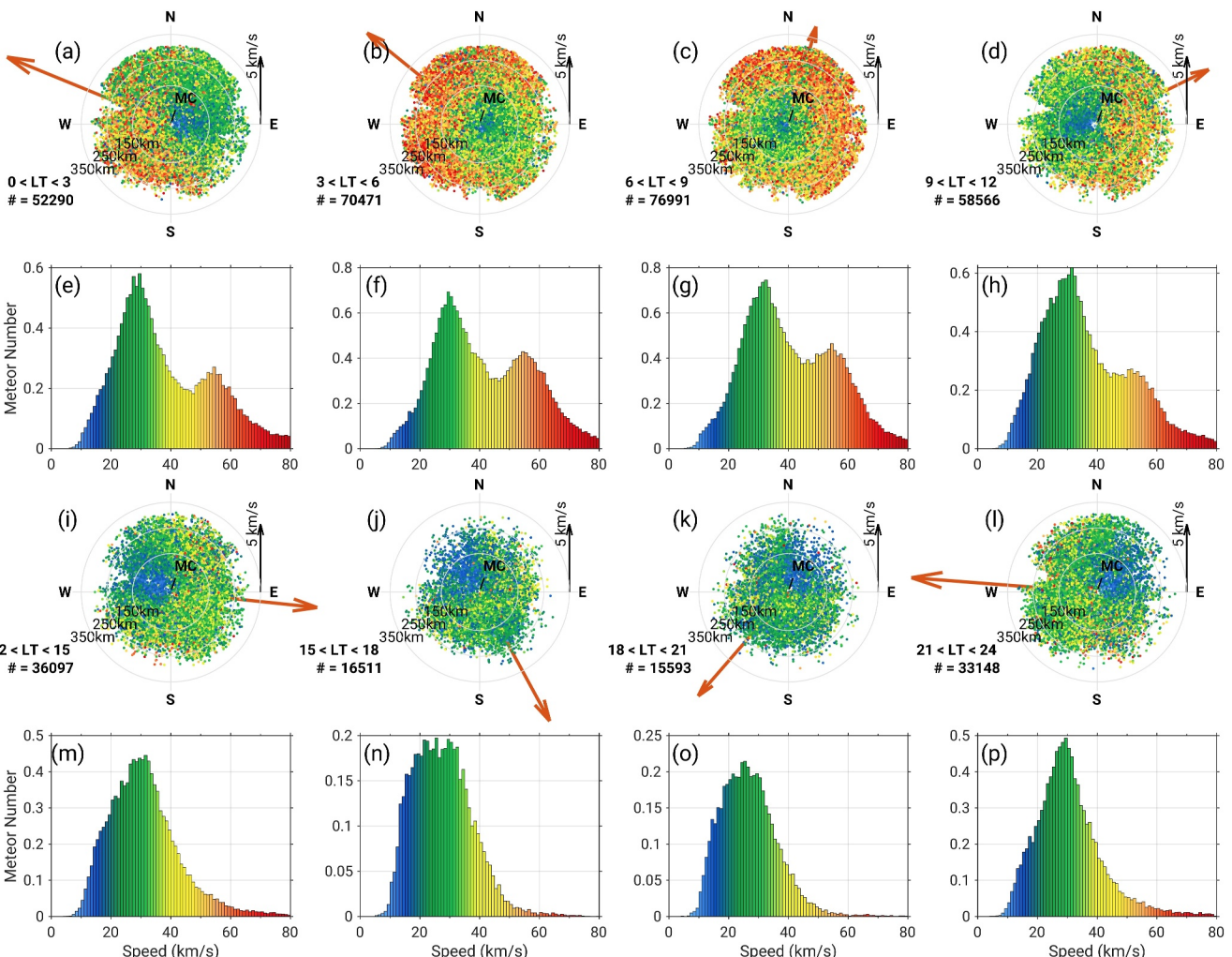


Figure 7. Distribution maps of meteor speeds as a function of horizontal distance and azimuth, sorted into 8 LT (Mengcheng local time, approximately UT+8 hr) intervals over a 30-day composite centered on 2 October 2022. In the first and third row maps, meteors are represented as colored points indicating speed, with color scales provided in the second and fourth rows; gray circles denote horizontal distances from 150, 250, and 350 km; the orange arrow is \mathbf{Q} , with a 5 km/s black quiver as its scale bar.

afternoon to evening (12–24 LT), the direction of \mathbf{Q} changes from the southeast (90° – 270°) to the southwest (180° – 270°). This phenomenon is similar to the change in the azimuth direction of the maximum meteor number and can be attributed to the self-rotation of the Earth. At sunrise, the fastest meteors originate from the north, which can be explained by the location of the MCMR in the Northern Hemisphere. On the other hand, meteors are the slowest at sunset. The meteor radar's changing direction, as the Earth rotates, relative to the local time, is responsible for the longitude difference from the sunrise. Consequently, the highest number of fast-moving meteors is observed coming from the north during the morning, while the opposite effect occurs in the evening.

The meteor speed distributions Figures 6 and 7 align with Sugar (1964), indicating that the meteor speed observed by meteor radars (i.e., the relative speeds between meteors and Earth) are influenced by the Earth's orbital speed around the Sun (approximately 30 km/s). Meteors approaching the Earth in the direction of its orbital motion may exhibit lower relative speeds due to the additive effect of Earth's motion, while those moving against this direction exhibit higher relative speeds. Meteors with very low relative speeds may not generate sufficient ablation to be detected by meteor radar. This interaction can lead to a two-peak distribution of meteor speeds when the meteor radar is located on the dayside, as both high-speed and low-speed meteors are observed. When the meteor radar is located on the night side, the effect of Earth's orbital speed is reversed, leading to a speed distribution where high-speed meteors are less likely to occur. This results in a single peak in the meteor speed distribution plot.

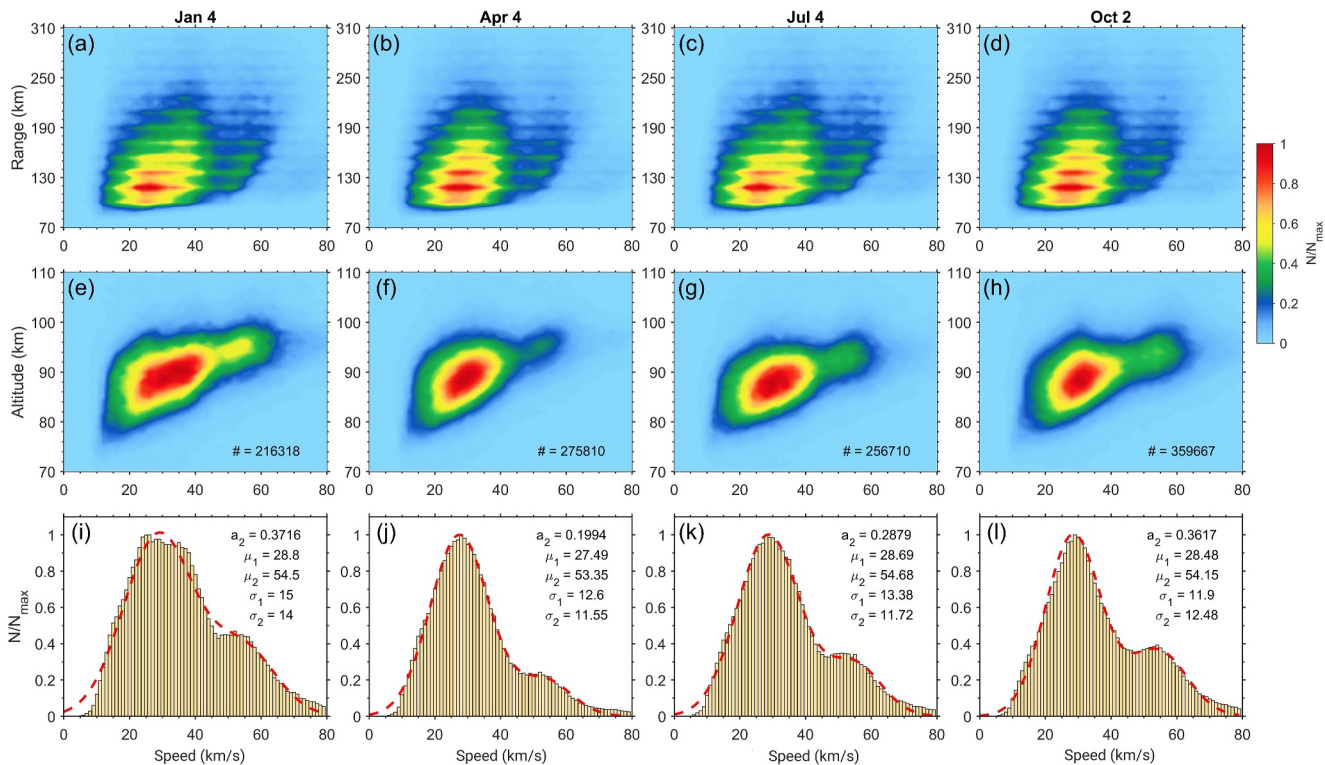


Figure 8. 30-day composite of meteor speed distribution centered on 4 January to 2 October 2022 (columns 1–4). Top row: meteor range-speed distribution. Second row: meteor altitude-speed distribution. Meteor counts are normalized to the maximum count, shown on the lower-right of the second row (e–h). Bottom row: histograms and double-Gaussian fitting curves for speed distribution, with calculated mean and standard deviation values shown.

4. Seasonal Variations of the Meteor Speed

Figure 8 illustrates the meteor range-speed distribution, meteor altitude-speed distribution, and meteor speed distribution over a 30-day period. Panels (a–d) indicate that meteor speed increases with range. Meteor height is derived from range, and Panels (e–h) demonstrate that for speeds below 50 km/s, the altitude-speed distribution reveals that the expected speed increases with altitude (e.g., Hocking, 2000; McKinley, 1961). According to meteor physics, meteors that are traveling quickly start to burn at high altitudes that are visible on the charts. There has been a localized rise in the number of meteors traveling at speeds of around 25 and 55 km/s (Holdsworth et al., 2008). This characteristic of the speed distribution may be linked to the heterogeneity in meteoric material dispersion close to the Earth's orbit. Comparing the joint distribution of meteors by speed and radiant is important to provide a more conclusive response to this query. It might suggest the existence of solitary meteoroid streams if close radiants exhibit high-speed meteors traveling at speeds of up to 55 km/s (Kalabanov et al., 2021).

Panels (i–l) in Figure 8 display speed histograms of meteor composite over a 30-day period, revealing a meteor speed distribution that resembles a superposition of roughly two Gaussian distributions. To determine the parameters of this distribution, we utilize the double-Gaussian fitting approach on the meteor distribution that has been normalized by its maximum count. As a result, the meteor speed distribution may be captured by describing the speed peaks and their corresponding widths as a function:

$$N_{\text{nor}}(t) = a_1 e^{-\frac{(v-\mu_1)^2}{\sigma_1^2}} + a_2 e^{-\frac{(v-\mu_2)^2}{\sigma_2^2}} \quad (2)$$

where a_1 and a_2 denote the amplitude of the lower and higher speed peak, μ_1 and μ_2 the lower and higher speed peak, and σ_1 and σ_2 the lower and higher speed width, respectively. Note that the speed peaks and widths are calculated using this function where a_1 is normalized to 1 to streamline calculations.

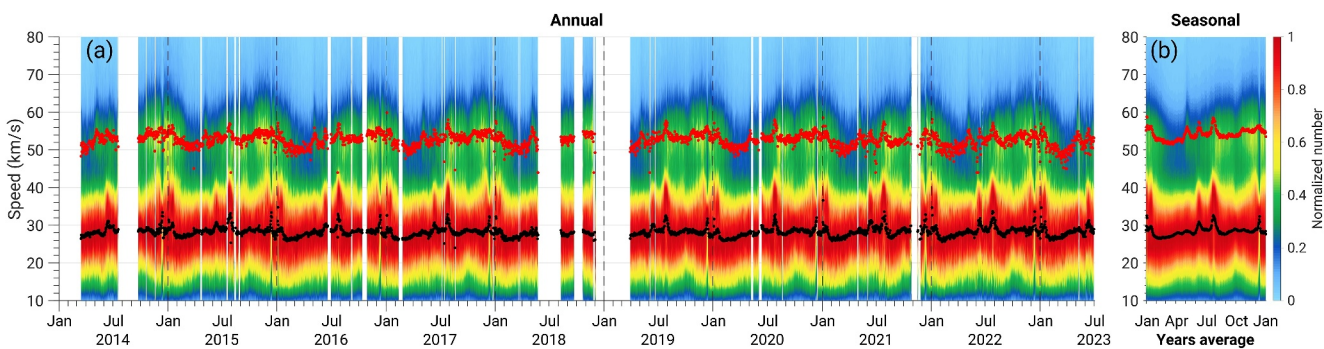


Figure 9. (a) Nine-year variations of daily meteor speed distributions, with red and black dots denoting daily lower speed peak (μ_1) and the higher speed peak (μ_2) observed by MCMR from April 2014 to June 2023. The color bar denotes the daily normalized meteor count. (b) Composite average of 9-year speed distributions for (a).

The higher speed peak, ranging from approximately 54 ± 1 km/s, and the lower speed peak, approximately 28 ± 1 km/s, exhibit seasonal variations patterns in Figure 8. The relative magnitude between the higher and lower speed peaks is measured by the ratio $R = a_2/a_1$. R is close to 0.36 near 4 January and 2 October, whereas it is close to 0.25 near 4 April and 4 July. This reveals that in comparison to the lower speed group, the higher speed group is weaker during the Northern Hemisphere's fall and winter than in spring and summer.

Following Equation 2, we utilize the double-Gaussian fitting approach to exhibit the seasonal changes in meteor speed distributions, including the daily high and lower speed peaks. Figure 9a displays 39.6 million meteor echoes captured from April 2014 to June 2023. The 9-year mean seasonal variation of the daily meteor speed distributions is shown in Figure 9b. In general, meteors with speeds between 20 and 40 km/s dominate throughout the year. From August to December, there is a peak region with a speed of about 54 km/s, which corresponds to a period of highly active meteor showers, as evident by Figure 2a.

Figures 8 and 9 provide insight into the two Gaussian distributions. The lower meteor speed Gaussian distribution with $\mu_1 \sim 28 \pm 1$ km/s, $\sigma_1 \sim 13 \pm 2$ km/s, while the higher one $\mu_2 \sim 54 \pm 1$ km/s, $\sigma_2 \sim 12 \pm 2$ km/s, as depicted in these figures. Seasonal variations are evident from the normalized numbers of both distributions, as shown in Figure 9. The lower Gaussian distribution has a semi-annual variation cycle, displaying a comparatively concentrated distribution in spring and fall, and a more scattered distribution in summer and winter. We have identified several speed ranges between 35 to 40 km/s during summer and winter, which correspond to meteor shower events and are shown in Figure 10. Moreover, the higher Gaussian distribution indicates the annual variation cycle, which is more prominent in spring and winter and weaker in summer and fall. Consequently, the value of a_2 is proportionately greater in Figures 8i and 8l as compared to Figures 8j and 8k, as the variance of the lower Gaussian distribution contrasts with that of the higher Gaussian distribution.

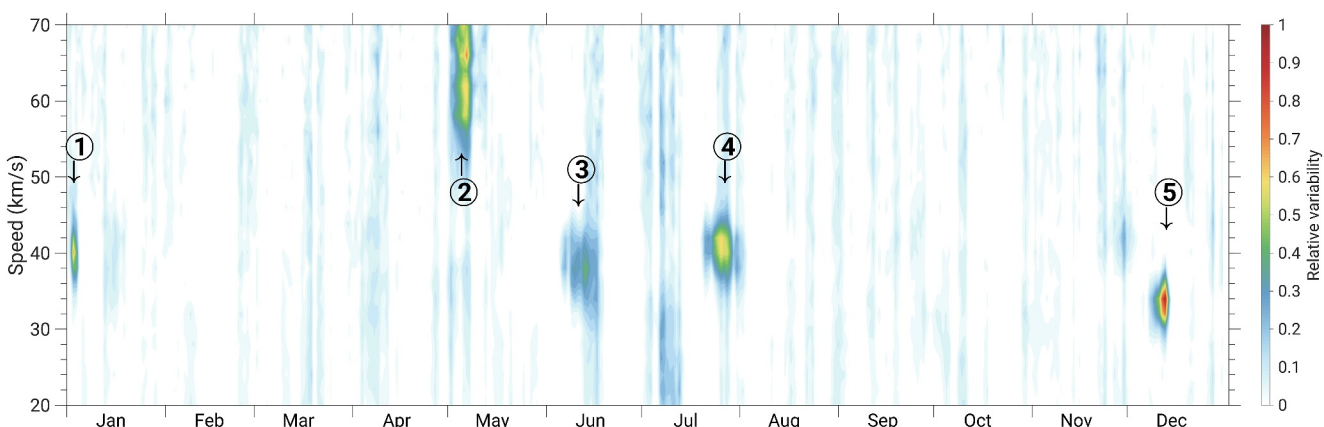


Figure 10. Seasonal variation of daily mean meteor speed distribution anomaly over 9 years from April 2014 to June 2023. The color bar denotes relative variability compared with the 30-day smoothed background. Numbered circles indicate meteor showers listed in Table 2.

These findings are consistent with the Davis meteor radar research indicating that lower and higher peaks occur around 25 and 55 km/s, respectively (Holdsworth et al., 2008), and the King Sejong Station meteor radar in 2017 demonstrating that peaks occur approximately at 30 and 50 km/s (Lee et al., 2022). McNamara et al. (2004) also show similar findings employing a sporadic meteor environment model and verifying it against radar data. In their study, the lower speed peak is about 20 km/s, while the higher speed peak is about 55 km/s.

In addition to the seasonal variation of meteor speed, as shown in Figure 9b, there are also several noticeable increases in the higher and lower speed peaks each year. The minimum for the lower peak occurs around February and August, while the maximum appears in June–July and December–January. In contrast, the higher peak reaches its maximum around May–December–January and its minimum around March. To ascertain the reasons for the formation of the two Gaussian distributions and their seasonal variations, it is necessary to investigate the sporadic sources of meteors. Six primary apparent “sources” of sporadic meteor radiants have been identified throughout the years. Campbell-Brown (2007) stated that apex sources move at high speeds, ranging from nearly 70 km/s to approximately 45 km/s as a result of their heliocentric speeds adding to the Earth's orbit speed. Conversely, the helion/anti-helion sources exhibit a wide range of speeds, differing between about 20(farthest from the apex) and 35 km/s (nearest to the apex). Unlike the helion and anti-helion sources, the north toroidal source moves at a uniform speed of 35 km/s.

Furthermore, Campbell-Brown (2008) suggested that the two speed peaks are mostly caused by several sources of sporadic meteors. Apex sources produce higher-speed meteoroids with speeds between 45 and 70 km/s, which typically have a smaller scale, while helion/anti-helion sources produce meteoroids with speeds between 20 and 35 km/s. J. P. Younger et al. (2009), P. T. Younger et al. (2009) explained that the low meteor counts observed in March were due to poor viewing geometry caused by the 2 sporadic meteor sources being below the local horizon (the southern apex and southern prograde apex source regions). However, their analysis revealed that during June and July, multiple sources, including southern apex and northern ones, above the horizon, combined with a change in atmospheric density structure, resulted in large counts.

As a result, the helion/anti-helion and apex sources both dominate the meteoroid speed distribution seen by MCMR during the fall and winter (see Figures 8a and 8d), whereas, during the spring and summer, only the helion/anti-helion sources dominate the meteoroid speed distribution (see Figures 8b and 8c). These observations were also clearly supported by Kero et al. (2012), who illustrated the radiant distribution of meteors' geocentric speed and radiant density of north and south apex sporadic meteor sources detected during the 2009–2010 MU radar head echo observation.

In addition to the sporadic meteor sources, meteor showers contribute to the variation in meteor speeds. Meteor showers occur when the Earth intersects with meteoroid streams that have similar speeds. Although meteoroid streams are unevenly distributed, resulting in varying shower intensities each year, showers occur annually between the same range of dates. Figure 9b demonstrates that local speed peak maxima are predominantly observed on specific days throughout the year. We also investigated whether these occurrences are related to meteor showers by calculating relative variability, obtained by subtracting the smoothed meteor background. Consequently, we discovered that these local maxima are indeed associated with meteor showers which are indicated by the relative variability in Figure 10. Specifically, the meteor count surpasses 45%–97% of the background count at the corresponding meteor shower event dates and speeds, causing the speed peaks to increase.

Table 2 lists the major meteor showers shown in Figure 10. It can be observed that there are comparatively small and narrow local maxima of speed peaks increasing during the shower periods, and the local maxima of the speed peaks of one to several days coincide with the peak activity dates of the major meteor showers. The magnitudes of the two speed peaks for the Quadrantids, Daytime Arietids, and southern Delta Aquariids, are higher than the 30-day smoothed background by approximately 2 km/s (H) & 2 km/s (L); 2.5 km/s (H) & 1.5 km/s (L); 2.5 km/s (H) & 2.5 km/s (L), respectively. However, during Eta Aquariids, only the higher peak reaches its local maximum, which is higher by approximately 2 km/s; during Geminids, only the higher peak reaches its local maximum, which is higher by approximately 2.5 km/s. On each plot, the approximation of the difference between the peak speeds of shower meteors and sporadic meteors is specified.

Figure 10 displays the distinctive characteristics of meteor activity, including shower meteors and sporadic meteors. The coherence of local maxima in the two speed peaks implies that some shower meteors have higher

Table 2

Characteristics of Meteor Showers That Are Identifiable and Numbered in Figure 10, Following the Shower Calendar of the International Meteor Organization (IMO) for the Year 2023 (IMO, 2022)

#	Shower	IAU code	Activity date	Peak activity date	V_∞ (km/s)	Type
1	Quadrantids	010 QUA	28 December to 12 January	04 January	41	H&L
2	Eta aquariids	031 ETA	20 April to 20 May	06 May	66	H
3	Daytime arietids	171 ARI	14 May to 24 June	07 June	38	H&L
4	Southern delta aquariids	005 SDA	12 July to 23 August	30 July	41	H&L
5	Geminids	004 GEM	04 December to 20 December	14 December	35	L

Note. The showers are listed in column 4 in order of their activity dates. Column 6 indicates the geocentric speeds (V_∞) of the meteor showers, while the final column points out the type of increased speed peaks during the meteor shower activities (H denotes the higher peak and L denotes the lower peak).

speeds, producing their ionized trails at higher altitudes than the sporadic background, consistent with the study about altitude distributions of meteor showers and sporadic meteors made by Lukianova et al. (2020). Moreover, the speed peaks of the meteors shown in Figure 10 exhibit considerably greater variations than those in Figure 8. This is due to the employment of the 30-day composite method in Figure 8, which mitigates the trend of variation.

As shown in Figure 11, we further investigated the active meteor shower count using the great circle technique (Jones & Jones, 2006), which uses the features of the radar-observed backscattered diffraction pattern to calculate the speeds of individual shower meteors. The Quadrantids in January, the Eta-Aquariids in April, the Arietids in June, the Southern Delta Aquariids in July, and the Geminids in December are the visible showers. It further confirmed the method used in Figure 10, which we use to distinguish shower meteors from the background. Although there were challenges in reliably deriving meteor speed distributions in periods with sparse meteor data or voids, and there might be slight discrepancies between peak activity dates, our observations generally align with the archived meteor shower calendar of the International Meteor Organization (IMO). As observed, there are clear interannual variations in the speed and count of meteor showers in Figure 11.

5. Conclusions

The USTC MCMR (33.36°N, 116.49°E) is located in the lower mid-latitudes of the Northern Hemisphere. It has been gathering data including meteor counts, range, azimuth, altitude, and speed since April 2014. This study yields the following points:

1. As expected, MCMR observations demonstrate the diurnal variation of meteor speed, azimuth peak, zenith peak, and the azimuthal direction of maximum meteor speed due to the Earth's rotation. Additionally, meteor counts exhibit a seasonal variation cycle, with the highest value recorded from September to October and the lowest in February.
2. The results show a strong correlation between speed and azimuth, with the azimuthal direction of maximum meteor speed shifting clockwise from the north in the morning to the south in the evening.
3. The meteor speed distribution resembles a superposition of two Gaussian distributions. The lower speed Gaussian distribution can be observed in the ~20 to ~40 km/s range, and the higher one, from ~45 to ~65 km/s. The lower Gaussian distribution demonstrates a semi-annual variation cycle, while the higher one shows an annual variation cycle. The two peak speeds of the Gaussian distribution were estimated using a double-Gaussian fitting approach. Generally, the peak speed of the lower Gaussian distribution is found to be around 28 km/s and indicates a semi-annual variation cycle. The peak speed of the higher Gaussian distribution, which is generally around 54 km/s, indicates an annual variation cycle.
4. We found a correlation between the seasonal variations in meteor speed peaks and the occurrence of meteor showers. The meteor counts surpassed 45%–97% of the background count at the corresponding meteor shower event dates and speeds, leading to an increase in speed peaks. The association of higher speed meteors with

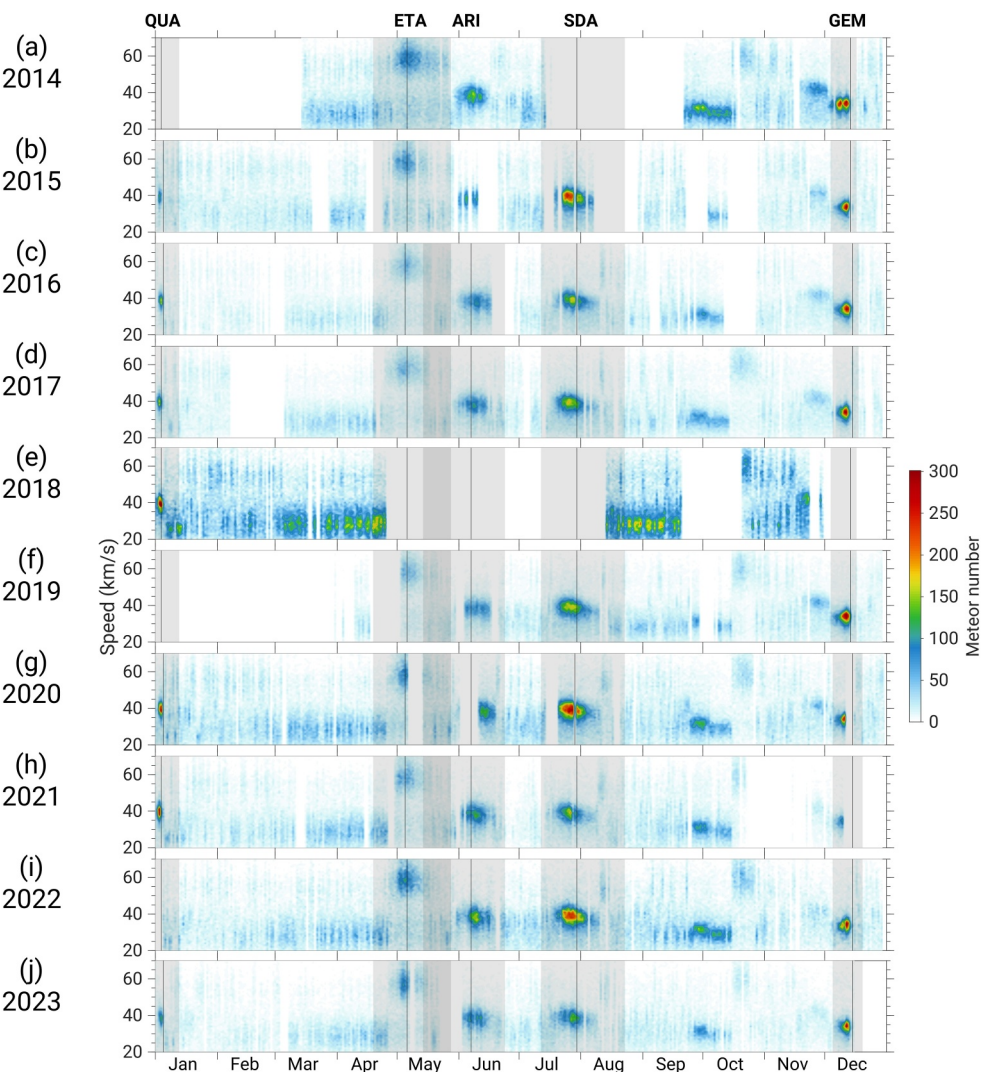


Figure 11. (a–j) Seasonal variation of daily meteor shower speed distribution from April 2014 to December 2023. The color bar denotes the meteor count of the shower. Shaded regions highlight shower activity dates, with vertical lines at peak activity dates, as reported by the International Meteor Organization shower calendar of each year (<https://www.imo.net/resources/calendar/>) and corresponding to columns 4 and 5 in Table 2. Minor data gaps, shown as white regions, are mainly due to site maintenance.

increased altitudes further supports the distinct dynamical and compositional characteristics of shower meteors compared to sporadic meteors. Additionally, by applying the great circle technique (Jones & Jones, 2006), we further confirm the crucial meteor shower events that showed a noticeable relative interannual variability.

More than 9 years of continuous observations using the MCMR are a supplement to previous shorter-duration meteoric studies using the backscatter meteor radars. The double-Gaussian fitting approach of the meteor speed provides a unique way to understand the seasonal variations of sporadic meteors and meteor showers. These findings underscore the role of meteor showers in influencing meteor speed distributions and altitudinal profiles, thus advancing our understanding of meteoric phenomena. This comprehensive data set and analysis can serve as a foundational reference for future meteoric studies.

Data Availability Statement

The Mengcheng meteor radar data presented in this work is available at Wu et al. (2023).

Acknowledgments

This work is supported by the National Key Technologies R&D Program of China (Grant 2022YFF0503703); the Project of Stable Support for Youth Team in Basic Research Field, Chinese Academy of Sciences (CAS; YSBR-018); the National Natural Science Foundation of China (Grant 42125402 and 42174183); the B-type Strategic Priority Program of CAS (Grant XDB41000000); the Chinese Meridian Project; the Fundamental Research Funds for the Central Universities; the Joint Open Fund of Mengcheng National Geophysical Observatory (MENGO-202407); and the Open Research for Innovation Challenge (ORIC) Program of X-Institute. This research was supported by the International Space Science Institute (ISSI) in Bern, through ISSI International Team project #23-580 “Meteors and phenomena at the boundary between Earth’s atmosphere and outer space.” We acknowledge the technical support of our radar systems by Chris Adami. We also express our gratitude to Jingnan Guo and Shiyuan Wang at USTC; Quanshui Zheng, Shaohua Xiang, Luping Xu, Jianxun Ren, and Liwen Jing at X-Institute for their valuable discussions.

References

- Bowman, M. R., Gibson, A. J., & Sandford, M. C. W. (1969). Atmospheric sodium measured by a tuned laser Radar. *Nature*, 221(5179), 456–457. <https://doi.org/10.1038/221456a0>
- Brown, P., Spalding, R. E., ReVelle, D. O., Tagliaferri, E., & Worden, S. P. (2002). The flux of small near-Earth objects colliding with the Earth. *Nature*, 420(6913), 294–296. <https://doi.org/10.1038/nature01238>
- Campbell-Brown, M. D. (2007). Directional variation of sporadic meteor activity and velocity. *Earth, Moon, and Planets*, 102(1–4), 79–84. <https://doi.org/10.1007/s11038-007-9152-8>
- Campbell-Brown, M. D. (2008). High resolution radiant distribution and orbits of sporadic radar meteoroids. *Icarus*, 196(1), 144–163. <https://doi.org/10.1016/j.icarus.2008.02.022>
- Carrillo-Sánchez, J. D., Gómez-Martín, J. C., Bones, D. L., Nesvorný, D., Pokorný, P., Benna, M., et al. (2020). Cosmic dust fluxes in the atmospheres of Earth, Mars, and Venus. *Icarus*, 335, 113395. <https://doi.org/10.1016/j.icarus.2019.113395>
- Cepelica, Z. (1992). Influx of interplanetary bodies onto Earth. *Astronomy & Astrophysics*, 263(1–2), 361–366.
- Cepelica, Z., Borovička, J., Elford, W. G., ReVelle, D. O., Hawkes, R. L., Porubčan, V., & Šimek, M. (1998). Meteor phenomena and bodies. *Space Science Reviews*, 84(3), 327–471. <https://doi.org/10.1023/A:1005069928850>
- Dou, X. K., Xue, X. H., Li, T., Chen, T. D., Chen, C., & Qiu, S. C. (2010). Possible relations between meteors, enhanced electron density layers, and sporadic sodium layers. *Journal of Geophysical Research*, 115(A6), A06311. <https://doi.org/10.1029/2009ja014575>
- Drolshagen, E., Ott, T., Koschny, D., Drolshagen, G., Schmidt, A. K., & Poppe, B. (2020). Velocity distribution of larger meteoroids and small asteroids impacting Earth. *Planetary and Space Science*, 184, 104869. <https://doi.org/10.1016/j.pss.2020.104869>
- Drolshagen, G., Koschny, D., Drolshagen, S., Kretschmer, J., & Poppe, B. (2017). Mass accumulation of Earth from interplanetary dust, meteoroids, asteroids and comets. *Planetary and Space Science*, 143, 21–27. <https://doi.org/10.1016/j.pss.2016.12.010>
- Galligan, D. P., & Baggaley, W. J. (2004). The orbital distribution of radar-detected meteoroids of the Solar system dust cloud. *Monthly Notices of the Royal Astronomical Society*, 353(2), 422–446. <https://doi.org/10.1111/j.1365-2966.2004.08078.x>
- Hindley, N. P. (2022). Analysis and Figure code for ACP publication ACP-2021-981 Hindley et al. (2022) [Software]. Zenodo. <https://doi.org/10.5281/zenodo.6819061>
- Hindley, N. P., Mitchell, N. J., Cobbett, N., Smith, A. K., Fritts, D. C., Janches, D., et al. (2022). Radar observations of winds, waves and tides in the mesosphere and lower thermosphere over south Georgia island (54°S, 36°W) and comparison with WACCM simulations. *Atmospheric Chemistry and Physics*, 22(14), 9435–9459. <https://doi.org/10.5194/acp-22-9435-2022>
- Hocking, W. K. (2000). Real-time meteor entrance speed determinations made with interferometric meteor radars. *Radio Science*, 35(5), 1205–1220. <https://doi.org/10.1029/1999rs002283>
- Hocking, W. K. (2004). Experimental Radar studies of anisotropic diffusion of high altitude meteor trails. *Earth, Moon, and Planets*, 95(1–4), 671–679. <https://doi.org/10.1007/s11038-005-3446-5>
- Holdsworth, D. A., Murphy, D. J., Reid, I. M., & Morris, R. J. (2008). Antarctic meteor observations using the Davis MST and meteor radars. *Advances in Space Research*, 42(1), 143–154. <https://doi.org/10.1016/j.asr.2007.02.037>
- Holdsworth, D. A., Reid, I. M., & Cervera, M. A. (2004). Buckland Park all-sky interferometric meteor radar. *Radio Science*, 39(5), RS5009. <https://doi.org/10.1029/2003rs003014>
- International Meteor Organization (IMO). (2022). The 2023 meteor shower calendar. In J. Rendtel (Ed.), *International Meteor Organization 2023 meteor shower calendar* (pp. 25–26). International Meteor Organization. Retrieved from <https://www.imo.net/files/meteor-shower/cal2023.pdf>
- Janches, D., Close, S., Hormaechea, J. L., Swarnalingam, N., Murphy, A., O’Connor, D., et al. (2015). The Southern Argentina Agile Meteor Radar Orbital System (SAAMER-Os): An initial sporadic meteoroid orbital survey in the southern sky. *The Astrophysical Journal*, 809(1), 36. <https://doi.org/10.1088/0004-637x/809/1/36>
- Janches, D., Hocking, W., Pifko, S., Hormaechea, J. L., Fritts, D. C., Brunini, C., et al. (2014). Interferometric meteor head echo observations using the Southern Argentina Agile Meteor Radar. *Journal of Geophysical Research: Space Physics*, 119(3), 2269–2287. <https://doi.org/10.1002/2013ja019241>
- Janches, D., Palo, S. E., Lau, E. M., Avery, S. K., Avery, J. P., Peña, S. d. l., & Makarov, N. A. (2004). Diurnal and seasonal variability of the meteoric flux at the South Pole measured with radars. *Geophysical Research Letters*, 31(20), L20807. <https://doi.org/10.1029/2004gl021104>
- Jones, J., & Jones, W. (2006). Meteor radiant activity mapping using single-station radar observations. *Monthly Notices of the Royal Astronomical Society*, 367(3), 1050–1056. <https://doi.org/10.1111/j.1365-2966.2006.10025.x>
- Jones, J., Webster, A. R., & Hocking, W. K. (1998). An improved interferometer design for use with meteor radars. *Radio Science*, 33(1), 55–65. <https://doi.org/10.1029/97rs03050>
- Kalabanov, S., Korotyshkin, D., Ishmuratov, R., Sherstykov, O., & Valiullin, F. (2021). Observations of meteor showers with the meteor radar of KFU. *Contributions of the Astronomical Observatory Skalnaté Pleso*, 51(3), 207–220. <https://doi.org/10.31577/caosp.2021.51.3.207>
- Kelley, M. C. (2004). A new explanation for long-duration meteor radar echoes: Persistent charged dust trains. *Radio Science*, 39(2), 1–6. <https://doi.org/10.1029/2003rs002988>
- Kero, J., Szasz, C., Nakamura, T., Meisel, D. D., Ueda, M., Fujiwara, Y., et al. (2012). The 2009–2010 MU radar head echo observation Programme for sporadic and shower meteors: Radiant densities and diurnal rates. *Monthly Notices of the Royal Astronomical Society*, 425(1), 135–146. <https://doi.org/10.1111/j.1365-2966.2012.21407.x>
- Lau, E. M., Avery, S. K., Avery, J. P., Janches, D., Palo, S. E., Schafer, R., & Makarov, N. A. (2006). Statistical characterization of the meteor trail distribution at the South Pole as seen by a VHF interferometric meteor radar. *Radio Science*, 41(4), 1–19. <https://doi.org/10.1029/2005rs003247>
- Lee, W., Lee, C., Kim, J. H., Kam, H., & Kim, Y. H. (2022). A modeling analysis of the apparent linear relation between mesospheric temperatures and meteor height distributions measured by a meteor radar. *Journal of Geophysical Research: Space Physics*, 127(1), e2021JA029812. <https://doi.org/10.1029/2021ja029812>
- Li, Y., Li, G., Hu, L., Zhao, X., Sun, W., Xie, H., et al. (2022). Observations of the October Draconid outburst at different latitudes along 120°E. *Monthly Notices of the Royal Astronomical Society*, 516(4), 5538–5543. <https://doi.org/10.1093/mnras/stac2589>
- Liu, L., Liu, H., Chen, Y., Le, H., Sun, Y.-Y., Ning, B., et al. (2016). Variations of the meteor echo heights at Beijing and Mohe, China. *Journal of Geophysical Research: Space Physics*, 121(1), 1117–1127. <https://doi.org/10.1002/2016JA023448>
- Lukianova, R., Kozlovsky, A., & Lester, M. (2020). Signatures of meteor showers and Sporadics inferred from the height distribution of meteor echoes. *Planetary and Space Science*, 189, 104981. <https://doi.org/10.1016/j.pss.2020.104981>
- Marino, J., Palo, S. E., & Rainville, N. (2022). First observations from a new meteor radar at McMurdo station Antarctica (77.8°S, 166.7°E). *Radio Science*, 57(11), 1–17. <https://doi.org/10.1029/2022rs007466>

- Maruyama, T., Kato, H., & Nakamura, M. (2008). Meteor-induced transient sporadic E as inferred from rapid-run ionosonde observations at midlatitudes. *Journal of Geophysical Research*, 113(A9), A09308. <https://doi.org/10.1029/2008JA013362>
- McKinley, D. W. R. (1961). *Meteor science and engineering*. McGraw-Hill.
- McNamara, H., Jones, J., Kauffman, B., Suggs, R., Cooke, W., & Smith, S. (2004). Meteoroid Engineering Model (MEM): A meteoroid model for the inner solar system. *Earth, Moon, and Planets*, 95(1), 123–139. <https://doi.org/10.1007/s11038-005-9044-8>
- Oppenheim, M. M., & Dimant, Y. (2006). Meteor induced ridge and trough formation and the structuring of the nighttime E-region ionosphere. *Geophysical Research Letters*, 33(24), L24105. <https://doi.org/10.1029/2006gl028267>
- Reid, I. M. (2024). Meteor Radar for investigation of the MLT region: A review. *Atmosphere*, 15(4), 505. <https://doi.org/10.3390/atmos15040505>
- Reid, I. M., Holdsworth, D. A., Morris, R. J., Murphy, D. J., & Vincent, R. A. (2006). Meteor observations using the Davis mesosphere-stratosphere-troposphere radar. *Journal of Geophysical Research*, 2006(A5), A05305. <https://doi.org/10.1029/2005JA011443>
- Reid, I. M., & Younger, J. (2016). 65 years of meteor radar research at Adelaide. In *International meteor Conference Egmond, The Netherlands, 2–5 June 2016*. 242. Retrieved from <https://hdl.handle.net/2440/109534>
- Rudraswami, N. G., Pandey, M., Genge, M. J., Fernandes, D., & Brownlee, D. (2021). Extraterrestrial dust as a source of bioavailable iron contributing to the ocean for driving primary productivity. *Meteoritics & Planetary Sciences*, 56(12), 2175–2190. <https://doi.org/10.1111/maps.13764>
- Ryabova, G. O., Asher, D. J., & Campbell-Brown, M. D. (Eds.) (2019). *Meteoroids: Sources of meteors on Earth and beyond* (p. 18). Cambridge University Press.
- Singer, W., Zahn, U. V., & Weiss, J. (2004). Diurnal and annual variations of meteor rates at the Arctic circle. *Atmospheric Chemistry and Physics*, 4(5), 1355–1363. <https://doi.org/10.5194/acp-4-1355-2004>
- Sugar, G. R. (1964). Radio propagation by reflection from meteor trails. *Proceedings of the IEEE*, 52(2), 116–136. <https://doi.org/10.1109/proc.1964.2801>
- Taylor, A. D., & Elford, W. G. (1998). Meteoroid orbital element distributions at 1 AU deduced from the Harvard Radio Meteor Project observations. *Earth Planets and Space*, 50(6–7), 569–575. <https://doi.org/10.1186/BF03352150>
- Wu, K., Yi, W., Xue, X., Reid, I., & Lu, M. (2023). Data of Mengcheng meteor velocity (version 0) [Dataset]. Zenodo. <https://doi.org/10.5281/zenodo.8002780>
- Yi, W., Reid, M., Xue, X., Younger, J. P., Spargo, A. J., Murphy, D. J., et al. (2017). First observation of mesosphere response to the solar wind high-speed streams. *Journal of Geophysical Research: Space Physics*, 122(8), 9080–9088. <https://doi.org/10.1002/2017JA024446>
- Yi, W., Xue, X., Reid, I. M., Murphy, D. J., Hall, C. M., Tsutsumi, M., et al. (2019). Climatology of the mesopause relative density using a global distribution of meteor radars. *Atmospheric Chemistry and Physics*, 19(11), 7567–7581. <https://doi.org/10.5194/acp-19-7567-2019>
- Yi, W., Xue, X., Reid, I. M., Murphy, D. J., Hall, C. M., Tsutsumi, M., et al. (2021). Climatology of interhemispheric mesopause temperatures using the high-latitude and middle-latitude meteor radars. *Journal of Geophysical Research: Atmospheres*, 126(6), e2020JD034301. <https://doi.org/10.1029/2020jd034301>
- Yi, W., Xue, X., Reid, I. M., Younger, J. P., Chen, J., Chen, T., & Li, N. (2018). Estimation of mesospheric densities at low latitudes using the Kunming meteor radar together with SABER temperatures. *Journal of Geophysical Research: Space Physics*, 123(4), 3183–3195. <https://doi.org/10.1002/2017JA025059>
- Yi, W., Xue, X. H., Zeng, J., Wang, J., Zhou, B., Ye, H., et al. (2023). Observation of MLT region winds and tides by the USTC Mengcheng meteor radar. *JUSTC*, 53(5), 0501. <https://justc.ustc.edu.cn/article/doi/10.52396/JUSTC-2022-0158>
- Younger, J. P. (2011). *Theory and applications of VHF Meteor Radar observations* (Ph.D. Thesis). University of Adelaide.
- Younger, J. P., Reid, I. M., Vincent, R. A., Holdsworth, D. A., & Murphy, D. J. (2009a). A southern hemisphere survey of meteor shower Radiants and associated stream orbits using single station radar observations. *Monthly Notices of the Royal Astronomical Society*, 398(1), 350–356. <https://doi.org/10.1111/j.1365-2966.2009.15142.x>
- Younger, J. P., Reid, I. M., Vincent, R. A., & Murphy, D. J. (2012). Meteor shower velocity estimates from single-station meteor radar: Accuracy and precision. *Monthly Notices of the Royal Astronomical Society*, 425(2), 1473–1478. <https://doi.org/10.1111/j.1365-2966.2012.21632.x>
- Younger, P. T., Astin, I., Sandford, D. J., & Mitchell, N. J. (2009b). The sporadic radiant and distribution of meteors in the atmosphere as observed by VHF radar at Arctic, Antarctic and equatorial latitudes. *Annals of Geophysics*, 27(7), 2831–2841. <https://doi.org/10.5194/angeo-27-2831-2009>